Published in final edited form as:

Cell Microbiol. 2013 March ; 15(3): 353–367. doi:10.1111/cmi.12051.

Myosin-X facilitates *Shigella*-induced membrane protrusions and cell-to-cell spread

Ellen A. Bishai[#1], **Gurjit S. Sidhu**[#1], **Wei Li**[1], **Jess Dhillon**[1], **Aparna B. Bohil**[2], **Richard E. Cheney**[2], **John H. Hartwig**[3], and **Frederick S. Southwick**[1,*]

[1]Department of Medicine, Division of Infectious Diseases, University of Florida College of Medicine, Gainesville, FL, USA.

[2]Department of Cell and Molecular Physiology, University of North Carolina, Chapel Hill, NC, USA.

[3]Department of Medicine, Division of Translational Medicine, Brigham and Women's Hospital, Harvard University, Boston, MA, USA.

[#] These authors contributed equally to this work.

Summary

The intracellular pathogen *Shigella flexneri* forms membrane protrusions to spread from cell to cell. As protrusions form, myosin-X (Myo10) localizes to *Shigella*. Electron micrographs of immunogold-labelled *Shigella*-infected HeLa cells reveal that Myo10 concentrates at the bases and along the sides of bacteria within membrane protrusions. Time-lapse video microscopy shows that a full-length Myo10 GFP-construct cycles along the sides of *Shigella* within the membrane protrusions as these structures progressively lengthen. RNAi knock-down of Myo10 is associated with shorter protrusions with thicker stalks, and causes a >80% decrease in confluent cell plaque formation. Myo10 also concentrates in membrane protrusions formed by another intracellular bacteria, *Listeria*, and knock-down of Myo10 also impairs *Listeria* plaque formation. In Cos7 cells (contain low concentrations of Myo10), the expression of full-length Myo10 nearly doubles *Shigella*-induced protrusion length, and lengthening requires the head domain, as well as the tail-PH domain, but not the FERM domain. The GFP-Myo10-HMM domain localizes to the sides of *Shigella* within membrane protrusions and the GFP-Myo10-PH domain localizes to host cell membranes. We conclude that Myo10 generates the force to enhance bacterial-induced protrusions by binding its head region to actin filaments and its PH tail domain to the peripheral membrane.

Introduction

Shigella flexneri is endemic in most developing countries and causes the significant mortality (Bennish and Wojtyniak, 1991; Kotloff *et al*., 1999). This Gram-negative rod is able to invade intestinal epithelial cells from the basolateral side by inducing cell ruffling using its type III secretion system. Upon escaping the vacuole and being released into the

[*]For correspondence. southf@epi.ufl.edu; Tel. (+1) 352 273 9511; Fax (+1) 352 392 6481. .

Supporting information Additional Supporting Information may be found in the online version of this article:

cytoplasm, *S. flexneri* goes on to usurp the host cell's actin machinery to form rocket tails. Actin assembly propels the bacteria within the cell and also allows direct spread to neighbouring cells via membrane protrusions. These protrusions push into adjacent cells, are ingested, and the life cycle is repeated in the new cell. The ability to form these structures allows the bacterium to avoid the extracellular milieu, and spread without detection by macrophages or antibodies (Finlay and Falkow, 1997). *S. flexneri* that are defective in the ability to form these membrane protrusions demonstrate a markedly reduced virulence in animal models (Sansonetti *et al*., 1991). Despite the major role these structures play in *S. flexneri* pathogenesis, little is known regarding the factor(s) and/or processes required to initiate and maintain bacteria containing membrane protrusions during *Shigella* infection.

Myosin-X (Myo10) is a recently discovered unconventional myosin that is found ubiquitously, though in low quantities, in many tissue types (Berg *et al*., 2000; Liu *et al*., 2012) and can utilize calmodulin-like protein (CLP), an epethelia-specific protein, as a light chain (Rogers and Strehler, 2001; Bennett *et al*., 2007). Overexpression of full-length Myo10 increased the number and length of conventional filopodia formed in Cos7 cells, and this increase required both the Myo10 head domain and elements within the tail domain (Berg and Cheney, 2002; Bohil *et al*., 2006; Plantard *et al*., 2010). Furthermore, by using a GFP-Myo10 construct, Myo10 was found to specifically localize to the tips of filopodia and to undergo forward and rearward movement along the filopodia (Berg and Cheney, 2002; Kerber *et al*., 2009; Watanabe *et al*., 2010). These observations suggest that Myo10 acts as an intrafilopodial motor. We now present the first report of this unconventional myosin being recruited by *S. flexneri* for efficient formation of bacteria containing membrane protrusions. Taking advantage of the large size of these membrane protrusions we have assessed the contribution of the multiple Myo10 structural domains to the generation of bacterial-induced membrane protrusions. We have also found that Myo10 localizes to *Listeria*-induced membrane protrusions and RNAi knock-down of this unconventional myosin markedly reduces the ability of both *Shigella* and *Listeria* to form plaques in confluent HeLa cells. We conclude that Myo10 plays a critical role in the cell-to-cell spread of both *Shigella* and *Listeria*.

Results

Myo10 localization in S. flexneri containing filopodia-like structures

Shigella's intracellular motility is dependent upon actin polymerization to generate the forces required to migrate to the peripheral cell membrane. Upon reaching the periphery, the bacteria often push the membrane outward to form distinct structures. In addition to actin, we explored the possibility that an actin–plasma membrane linking protein might be involved in formation of these bacteria containing membrane protrusions. One class of actin-binding proteins is unconventional myosin, and these proteins are often implicated in powering specific processes in conjunction with actin (Berg *et al*., 2001). One unconventional myosin thought to link actin to the plasma membrane and also known to stimulate filopodia formation in uninfected cells is myosin-X (Myo10). We utilized a specific polyclonal anti-Myo10 antibody to examine this protein's localization in *Shigella*-infected HeLa cells and discovered that Myo10 concentrated within each bacterium-

containing peripheral membrane protrusion (Fig. 1A and B). To assure that bacteria were in membrane projections cells were stained with anti-Ezrin, a protein that concentrates in peripheral membrane. As shown in Fig. 1C, Myo10 did not localize to bacteria within the host cell cytoplasm. These images are representative of multiple images. Of 51 *Shigella* within the host cell cytoplasm, 0 stained for Myo10. Of 55 *Shigella* localized to membrane protrusions 38 clearly stained for Myo10. These differences were highly significant ($P < 0.0001$).

To gain further insight into the nature of the cytoskeletal structure of *Shigella*-induced membrane projections we performed freeze-fractured rotary shadowed electron micrographs of infected HeLa cells. As shown in Fig. 2A and B, *Shigella* induce the assembly of an extensive network of microfilaments directly behind many of the bacteria. Previous work has shown that the assembly of actin filaments drives the bacteria through the cytoplasm until they eventually reach the peripheral membrane where they form outward projections. Using anti-Myo10 immunogold labelling we found that Myo10 localized along the sides and rear of bacteria within these membrane projections (Fig. 2C and D). In bacteria forming extensive cytoskeleton tails Myo10 was observed to also concentrate in the cytoskeleton, particularly near the rear of the bacterium (Fig. 2D).

To further explore the localization of Myo10, PtK2 cells were transfected with full-length green fluorescent protein-tagged (GFP)-Myo10 and then infected with *Shigella*. GFP-Myo10 was found to localize along the sides of *Shigella* within the filopodia-like structures, as well as in the actin tails (Fig. 3). When the protein localized around bacteria in membrane protrusions it concentrated in discrete clusters and also concentrated in the peripheral membranes in areas not containing bacteria in the tips of small host cell filopodia, as previous described (Berg and Cheney, 2002) (arrowheads, Fig. 3).

Analysis of time-lapse video revealed that the GFPMyo10 clusters adjacent to the bacteria within membrane protrusions cycled along the sides of the bacteria in both a forward and backward direction. Note the movement of GFP-Myo10 in the upper right bacterium with double arrows, and adjacent to the bacterium in the low centre, single arrow of Fig. 3. The mean forward velocity was 0.079 ± 0.006 μm s^{-1} (SEM, $n = 16$) and the mean backward velocity was 0.055 ± 0.006 μm s^{-1} (SEM, $n = 18$). As the Myo10 cycled, the bacteria containing protrusions elongated and the narrow stalk connecting the bacterium to the cell progressively lengthened with a mean velocity of 0.039 ± 0.02 μm s^{-1} (SEM, $n = 20$) (see supplementary Video S1). In transfected cells a high percentage of bacteria in membrane protrusions had visible clusters of GFP-Myo10 (44/51 bacteria containing membrane structures or 86%). Identical localization of GFP-Myo10 was observed in transfected HeLa cells following *Shigella* infection (data not shown).

Effects of reducing of endogenous Myo10 levels on S. flexneri membrane protrusion formation and cell-to-cell spread in HeLa cell monolayers

To further explore the functional importance of Myo10 for *Shigella*-induced membrane protrusions, we utilized Myo10 siRNA knock-down, and compared the lengths of *Shigella*-induced filopodia-like structures in cells treated with non-targeted siRNA. Western blots of HeLa cells 3 days after siRNA treatment showed a >90% reduction of Myo10 (insert Fig.

4A). As assessed by fluorescence microscopy of cells transfected with RFP-CAAX as shown in Fig. 1, knock-down of Myo10 reduced the mean length of membrane protrusions by 25% as compared with untargeted siRNA (Fig. 4A, bar graph). Although knock-down of Myo10 significantly shortened the length ($P < 0.0001$), reductions in Myo10 had no significant effect on the number of *Shigella*-induced protrusions per cell (control siRNA 126 filopodia/67 infected cells or 1.9 membrane protrusions per cell; Myo10 siRNA 119 filopodia/67 infected cells or 1.8 membrane protrusions per cell, $P = 0.83$). Confocal microscopy of formalin-fixed cells revealed that the *Shigella*-induced membrane protrusions lay flat in a single narrow focal plane, allowing accurate measurement of their lengths in two-dimensional planes (data not shown).

Scanning electron microscopy was utilized to further assess the effects of reducing Myo10 levels on membrane protrusion formation. As shown in Fig. 4B–D, HeLa cells transfected with control siRNA supported the formation of bacteria-laden membrane protrusions with narrow stalks (mean stalk width at the base of the filopodia = 0.22 ± 0.02 μm, SEM $n = 54$). As previously described in uninfected HeLa cells, *Shigella*-infected cells also supported the formation of large numbers of smaller dorsal filopodia (Bohil *et al*., 2006), indicating that the pathways mediating normal filopodia formation remained intact. The widths of these filopodia bases were much smaller than *Shigella* containing filopodia-like structures (widths varied from 0.05 to 0.07 μm, see Fig. 4C and D).

When HeLa cells were transfected with siRNA specifically directed against Myo10, a marked change in the morphology of *Shigella*-associated membrane protrusions was consistently observed. The bases of the majority of these bacteria laden membrane protrusions were markedly thickened and maintained the approximate diameter of the bacteria throughout their full length (Fig. 4B, E and F) (mean stalk width 0.50 ± 0.03 μm, SEM $n = 68$) was significantly wider than infected control cells, $P < 0.0001$. In control cells only 13/54 (24%) of the filopodia-like structures demonstrated a thick base, while siRNA Myo10 treatment resulted in 59/68 (86%) of the protrusions forming thick bases, a highly significant difference ($P < 0.0001$). Scanning EM also allowed a more accurate assessment of the length of these structures, and these measurements confirmed that reduction in Myo10 in HeLa cells was associated with a 24% reduction in the length of the bacteria-containing membrane protrusions (control mean length 11.3 ± 0.5 μm, SEM $n = 54$ versus RNAi Myo10 mean length 8.6 ± 0.4 μm, SEM $n = 68$, $P = 0.0008$) confirming our light microscopic findings.

Because the formation of membrane protrusions is critical for *Shigella* cell-to-cell spread, host proteins of functional importance for the formation of these structures would be expected to affect the ability of *Shigella* to spread to adjacent cells (Sansonetti, 2001). To test this expectation we examined the ability of Myo10 siRNA knock-down cells to support bacterial cell-to-cell spread utilizing a cultured cell monolayer plaque assay (Oaks *et al*., 1985). *Shigella*-infected HeLa cell monolayers treated with Myo10 siRNA demonstrated a marked decrease in the plaque number (Fig. 5A and B, 1/3 of controls), and plaque two-dimensional area (Fig. 5A and C, relative area < 1/2 of controls) resulting in a >80% overall decrease in the area of cell monolayer necrosis as compared with infected HeLa cell monolayers treated with control siRNA.

To assure that Myo10 knock-down did not affect bacterial entry into host cells, the number of intracellular bacteria per HeLa cell was determined by microscopy following washing and formalin fixation.An identical mean number of intracellular bacteria was observed at 2 h post infection in HeLa cells treated with untargeted siRNA and Myo10 siRNA (control: 9.8 ± 1.5 bacteria per cell, SEM n = 29 cells versus Myo10 siRNA: 9.8 ± 1.1 bacteria per cell, SEM n = 32 cells). The absence of any inhibition of bacterial entry by Myo10 RNAi was further confirmed by culturing lysed infected HeLa cell monolayers at 2 h after the start of infection (control: mean colony count 2.65×10^3 versus Myo10 siRNA: 3.5×10^3, n = 2 experiments).

Effects of Myo10-truncated constructs on the localization and enhancement of Shigella-*induced membrane protrusions*

To explore the roles of specific regions of Myo10 in membrane protrusion formation we utilized a series of truncated mutants (Fig. 6A). We first compared the ability of GFPMyo10-HMM to localize to *Shigella*-induced membrane protrusions. GFP-Myo10-HMM consists of the head, neck and alpha-helical domain, but lacks the remainder of the tail (this construct is also known as GFP-Myo10 ΔPH-MyTH4-FERM). As observed with full-length Myo10, GFP-Myo10-HMM concentrated on the sides of bacteria within membrane protrusions (Fig. 6B), forming clusters that cycled forward and backward with the same velocities as the full-length construct (forward velocity: 0.08 μm s^{-1} ± 0.03 SEM n = 14; backward velocity: 0.06 μm s^{-1} ± 0.02 n = 12). However unlike of full-length Myo10 that localized to both membranes and along the sides of bacteria within membrane protrusions, the GFP-Myo10-HMM truncate only concentrated along the sides of bacteria within the membrane protrusions, but not to peripheral membranes. In 50 images containing 83 bacteria containing membrane protrusions, in all instances HMM localized as shown in Fig. 6B. In contrast, a GFP construct lacking the motor domain (GFP-Myo10-tail; Fig. 6C) failed to localize specifically along the sides of bacteria, but rather concentrated along the entire length of the membrane protrusions (see arrows Fig. 6C), as well as concentrating in other regions containing peripheral membrane (observed in 108 of 108 transfected cells). These findings indicate that the head, neck predicted helical region are sufficient for proper localization of Myo10 along the sides of the bacteria within membrane protrusions, while the tail region links Myo10 to the protrusion's peripheral membranes.

To further determine which regions of the tail bind to the peripheral membrane, the localization of two additional GFP tail constructs was examined. The tail domain can be divided into three regions (Fig. 6A). The FERM domain contains a consensus sequence that provides a potential link to integral membrane proteins such as integrins (Zhang *et al*., 2004). The MyTH4 domain is found in a number of unconventional myosins and this domain of Xenopus Myo10 has been shown to bind microtubules (Weber *et al*., 2004; Kerber and Cheney, 2011; Wei *et al*., 2011). The tail also contains three PH domains that have been implicated in binding to phosphoinositides and can associate with the plasma membrane (Mashanov *et al*., 2004; Plantard *et al*., 2010; Lu *et al*., 2011; Umeki *et al*., 2011). We found that the GFP-tail-PH domain (Fig. 6A) concentrated along peripheral membranes in an identical pattern to the full-length tail (compare Fig. 6D with C) (observed in 32 of 32 transfected cells), while the GFP-MyTH4-FERM tail construct diffusely

distributed throughout the cytoplasm and heavily concentrated in the host cell nucleus (Fig. 6E) (observed in 37 of 37 transfected cells), indicating that the tail-PH domains are primarily responsible for linking Myo10 to the peripheral membrane.

Next we explored the function effects of deleting specific regions of Myo10 by comparing the ability of these different Myo10 constructs to potentiate *Shigella*-induced membrane protrusion formation in Cos7 cells. Unlike HeLa cells, COS7 cells lack filopodia on their dorsal surfaces (Bohil *et al*., 2006). We reasoned that increasing the content of full-length Myo10 by transfection of GFP-full-length Myo10 should enhance *Shigella*-induced membrane protrusion formation, and that truncated constructs containing the primary functional domains of Myo10 would also be expected to enhance bacteria-induced membrane protrusion formation, while constructs missing critical functional domains would not. As predicted, full-length Myo10 resulted in a near doubling of bacterial-induced membrane projection length in Cos7 cells, (mean of 6.1 ± 0.5 μm, SEM, $n = 94$ for cells transfected with GFP alone versus 10.9 ± 0.8 μm, $n = 110$ for GFP-Myo10-transfected cells, see Fig. 7A). This increase in length was highly statistically significant ($P < 0.0001$). Increased levels of full-length Myo10 had no significant effect on the number of bacteria-induced membrane protrusions (GFP = 94 protrusions/147 cells = 0.64 protrusions/cell versus full-length Myo10 = 110 protrusions/155 cells or 0.71 bacteria containing protrusions per cell $P = 0.34$).

Cells were next transfected with GFP-Myo10-ΔFERM. This construct contains the head domain, as well as the entire tail domain with the exception of the carboxyterminal FERM domain (see Fig. 6A). Transfection resulted in an increase in membrane protrusion length comparable to the full-length GFP-Myo10 construct (see Fig. 7A). Transfection with GFP-Myo10-ΔMyTH4FERM missing both the FERM-binding domain and the myosin tail homology 4 domain (MyTH4), also significantly increased protrusion length, $P = 0.001$ (see Fig. 7A), although to lesser extent than full-length or Myo10-ΔFERM. Transfection with the Myo10 tail, which lacks the head region, failed to increase protrusion length (Fig. 7A) and the same outcome was observed after transfection with GFP-Myo10-HMM. Co-transfection with the membrane marker RFP-CAAX revealed that the morphology of the membrane protrusions in cells transfected with Myo10-HMM was distinctly different than infected Cos7 cells transfected with the full-length construct. The bacteria containing structures were short and had thick stalks in Myo10-HMM-transfected cells, while the membrane projections in cells expressing the full-length Myo10 were longer, and had very thin stalks (Fig. 7B).

Role of Myo10 in Listeria-induced membrane protrusions and Listeria cell-to-cell spread

Listeria monocytogenes like *Shigella* forms membrane protrusions in order to spread from cell to cell. To determine if Myo10 also played a role in *Listeria* pathogenesis we first performed immunofluorescence localization with anti-Myo10 antibody. As observed with *Shigella*, Myo10 colocalized with bacteria within membrane protrusions (62 of 64 noted to staining with anti-Myo10) (Fig. 8A and B), but did not localize to bacteria within the host cell cytoplasm (46/49 intracellular bacteria demonstrated no anti-Myo10 staining). RNAi knock-down of Myo10 reduced *Listeria*-induced over all plaque formation area by nearly

half as compared with infected control (Fig. 8C) confluent HeLa cell monolayers. Knock-down of Myo10 did not affect the number of intracellular bacteria found in HeLa cells 2 h after infection (colony counts of infected lysed control monolayer: $7.33 \pm 0.68 \times 10^3$, SEM $n = 3$, control versus Myo10 RNAi: $8.9 \pm 2.9 \times 10^3$, SEM $n = 3$) indicating that loss of Myo10 did not interfere with the initial entry of *Listeria* into host cells. These findings indicate that Myo10 facilitates cell-to-cell spread in both *Listeria* and *Shigella*.

Discussion

One of the primary clinical characteristics of *Shigella* enterocolitis is bloody diarrhoea. The loss of blood into the colon results from the formation of discrete ulcerations in the colonic mucosa, and plaque formation in tissue culture monolayers is a consistent finding for all pathogenic strains of *Shigella* (Oaks *et al*., 1985). These ulcerations are the consequence of *Shigella's* ability to form membrane protrusions that push into adjacent cells. These bacteria containing protrusions are ingested by adjacent mucosal cells allowing the bacteria to spread from cell to cell without coming in contact with the humoral immune system or extracellular antibiotics. To date there have been no studies exploring the molecular components of these *Shigella*-induced membrane protrusions.

Little is known about how the membrane protrusions are formed during *Shigella* infection. Some clues may be derived from the much smaller conventional filopodia formed by most cells during movement. As cells move they form small filopodia to explore their environment, and following filopodia formation, broad lamelipodia subsequently expand the leading edge of the cell. There has been considerable interest in exploring how filopodia in uninfected cells are formed (Gupton and Gertler, 2007). Myo10 has been identified as a ubiquitous unconventional myosin that when overexpressed in Cos7 cells can induce the formation of filopodia (Berg and Cheney, 2002; Bohil *et al*., 2006). There has been considerable debate about how Myo10 enhances filopodia formation. The head, neck and alpha-helix construct (Fig. 6A) is sufficient for localization to filopodia (Berg and Cheney, 2002). Myo10 lacking the motor domain fails to localize to filopodia tips (Berg and Cheney, 2002), and neither GFP-Myo10-HMM or headless GFP-Myo10 induces filopodia formation, indicating that both the head and elements of the tail are required for Myo10-induced filopodia formation (Bohil *et al*., 2006). Myo10 represents one of several unconventional myosins that contains both a MyTH4 (myosin tail homology 4) and a FERM (band 4.1, ezrin, radixin, moesin) domain; however, removal of the FERM domain has no effect on the ability of Myo10 to induce dorsal filopodia formation in Cos7 cells (Zhang *et al*., 2004; Watanabe *et al*., 2010). Myo10 is the only unconventional myosin in vertebrates that possess multiple PH domains, and there is evidence that its activity is mediated by PI3-kinase (Cox *et al*., 2002; Plantard *et al*., 2010; Umeki *et al*., 2011)

We now show for the first time that Myo10 is a component of *Shigella*-induced and *Listeria*-induced membrane protrusions. Because *Shigella* induces the formation of membrane protrusions that are much larger than the filopodia generated by uninfected cells (*Shigella*-induced membrane structures: 5–30 μm in length and, at the bacteria containing tip, 0.5 μm width versus uninfected cell filopodia: 1–2 μm length and <0.1 μm width), we were able to more readily visualize GFP-Myo10 chimeras in these structures, and assess their functional

effects by light microscopy, as well as electron microscopy. Unlike conventional filopodia that form less frequently when Myo10 content is reduced, siRNA Myo10 treatment had no effect on the number of membrane protrusions induced by *Shigella*. Therefore, *Shigella* possesses the machinery to initiate the formation of these structures, and does not appear to require Myo10 for this first step. This characteristic simplifies the functional characterization of Myo10 in our experiments. The *Shigella* model has allowed us to strictly explore the effects of Myo10 on membrane protrusion length and overall structure, and to more fully characterize how Myo10 enhances the elongation of the bacteria-induced membrane protrusions, as well as to assess its role in *Shigella* cell-to-cell spread.

As observed for filopodia formed in uninfected cells, the head–neck–alpha-helix region is responsible for localizing Myo10 to the actin filaments formed on the sides of *Shigella*, and the rate of forward and backward movement of the Myo10 clusters of full-length Myo10 and the head–alpha-helix construct are the similar to Myo10 movement observed in filopodia formed in uninfected cells (see Fig. 3 and supplemental video) (Watanabe *et al*., 2010). The forward motion in all likelihood represents movement of the myosin heads towards the tip of the membrane protrusions, in the direction of the barbed ends of the actin filaments (see Fig. 9). Also as observed for filopodia in uninfected cells, expression of full-length Myo10 increases the length of *Shigella*-induced membranes protrusions, while expression of the head domain does not (Berg and Cheney, 2002) (see Fig. 7A).

Expression of Myo10 mutant proteins lacking different regions of the tail domain have now revealed the functional domains that are important for harnessing the force generated by the myosin head to elongate these membrane protrusions. Our studies demonstrate that the PH domain of the tail links the head region to the peripheral membrane, and is required to enhance *Shigella*-induced membrane projection elongation (see Fig. 7A). Although ERM proteins have been shown to play an important role in *Listeria*-induced protrusions (Pust *et al*., 2005), the loss of the FERM domain did not impair the ability of Myo10 to increase the length of *Shigella*-induced membrane protrusions (see Fig. 7A). Based on our experiments the loss of the PH domains renders Myo10 incapable of facilitating the elongation of *Shigella* mediated membrane protrusions. The combined PH1, 2 and 3 domains found in the Myo10 tail possess the ideal characteristics to serve as a membrane linker. These domains bind to the inner leaflet of the plasma membrane with high affinity and demonstrate minimal lateral diffusion (Mashanov *et al*., 2004). The PH2 domain of the Myo10 tail also plays an important role in the activation Myo10 motor function (Umeki *et al*., 2011). These PH domains could also serve to bind and transport another as yet unidentified component important for membrane protrusion formation and facilitation of cell-to-cell bacterial spread.

Based on our findings we propose a model for how Myo10 facilitates *Shigella*-induced membrane protrusion lengthening (see Fig. 9). As *Shigella* is propelled through the cytoplasm it eventually encounters the confining peripheral cell membrane. As the force of actin assembly pushes the membrane outwardly, the head of Myo10 binds to the actin filaments formed along the sides of the bacterium. Simultaneously Myo10 pH tail domain binds to the inner regions of the peripheral membrane linking the actin filaments associated with bacterium to the protruding host cell peripheral membrane. Myo10 is then activated and in the presence of ATP shifts its head angle from 90° to 45° moving the membrane

towards the tip of the bacterium. As the heads processively cycle they transport host cell membrane towards the membrane tip, enhancing elongation of the membrane protrusion (see Fig. 9). It is also possible that Myo10 binds some as yet unidentified component and transports it to the tip of the membrane projections and this component could play a key role in cell-to-cell spread of the bacteria, and we are presently searching for such a component.

This model can explain the dramatic change in the membrane protrusion morphology when Myo10 content is markedly reduced by siRNA; as predicted the membrane protrusions were shorter. With the loss of Myo10 force to move peripheral membrane towards the tip of the bacteria, *Shigella* has to rely on actin assembly alone to lengthen the protrusions, and this condition would require larger numbers of actin filaments in the stalk and our model predicts the stalks should remain thicker (compare left image to right image, Fig. 9) as observed after Myo10 RNAi treatment (Fig. 4B, E and F). Future experiments designed to assess the biophysical properties of bacteria containing membrane protrusions before and after Myo10 silencing should provide additional insights into how Myo10 facilitates membrane protrusion elongation.

Loss of Myo10 markedly impairs *Shigella* and *Listeria* cell-to-cell spread, resulting in a greater than 80% reduction in plaque area of monolayers infected by *Shigella* and a 50% reduction when infected by *Listeria* (Figs 5 and 8) emphasizing the critical role of Myo10-induced protrusions in *Shigella* and *Listeria* pathogenesis. This profound effect on cell-to-cell spread along with our time-lapse video image suggesting that bacteria containing membrane protrusions from adjacent cells may attract Myo10 (see supplemental video right mid-cell region) raise the possibility that Myo10 could also facilitate cell-to-cell spread by enhancing bacterial-membrane protrusion phagocytosis. This possibility is presently being explored. In addition Myo10 is known to be important for the formation of adherens junctions (Liu *et al*., 2012) and loss of Myo10 would be expected to impair cell–cell junction formation, a condition that could further impair the ability of *Shigella* and *Listeria* to spread from cell to cell.

Given the vital role of bacterial-induced membrane protrusions not only for the spread of *Shigella* and *Listeria*, but also for the spread of other intracellular bacteria including Rickettsia, and Mycobacteria, we feel that membrane protrusions produced by intracellular bacteria deserve a specific name. We propose to call them trans-podia emphasizing their central role in transporting pathogens from cell to cell. It will be of interest to characterize the role of Myo10 in these other bacteria, and to assess the function of other actin-regulatory proteins in the formation of these dynamic structures.

Experimental procedures

Cell cultures and bacterial strains

HeLa (human cervical cancer) cells, PtK_2 (kangaroo rat kidney) cells and Cos7 (African green monkey kidney) cells were maintained at 37°C and 5% CO_2 in Dulbecco's modified essential media (DMEM) containing 10% fetal bovine serum and 5% penicillin/streptomycin antibiotic solution (DMEM complete). *S. flexneri* strain 2457T, a virulent strain of serotype 2a (Wei *et al*., 2003), was a kind gift from Dr Marcia Goldberg, Harvard

Medical School. Individual bacterial colonies were selected from a tryptic soy agar or brain heart infusion agar plate containing 0.01% Congo Red dye to ensure bacterial virulence (Meitert *et al*., 1991). Colonies were inoculated into tryptic soy broth (TSB) or brain heart infusion (BHI) and were grown overnight in a shaker at 37°C. The next day, a diluted culture was made from the overnight culture and allowed to grow to an OD_{600} between 0.600 and 0.800 to ensure optimal expression of the outer-membrane protein, IcsA (Goldberg *et al*., 1994; Stevens *et al*., 2006).

Intracellular S. flexneri *infection*

Shigella flexneri invasion of semiconfluent cell monolayers was performed as described previously with some modifications (Zeile *et al*., 1996). Briefly, bacteria in log phase were spun down, washed and resuspended in 1× phosphate-buffered saline (PBS). Bacteria were then added to HeLa cells grown on 35 mm culture dishes at an moi of 50 bacteria per cell and subsequently centrifuged at 500 *g* for 15–30 min to allow for bacterial adhesion and entry. Culture dishes were then incubated for another 30–90 min at 37°C and 5% CO_2 to allow for initiation of bacterial actin-based motility and membrane protrusion formation. Extracellular bacteria were then removed by washing cells with 1× PBS. Media containing gentamicin at a concentration of 10 μg ml^{-1} was then added back to the culture dishes to prevent growth of extracellular bacteria and cells were incubated at 37°C and 5% CO_2 for 10–15 min before being viewed via video microscopy.

Plaque assays

The plaque assay protocol was carried out as previously described (Oaks *et al*., 1985), with some modifications. Briefly, HeLa cells were grown to confluency in six-well plates containing appropriate media at 37°C and 5% CO_2. *Shigella* were added to cell monolayers at an moi of five bacteria per cell. Plates were then incubated at 37°C and 5% CO_2 for 90 min. During this adsorption or attachment period, plates were rocked back and forth every 30 min to ensure equal distribution of bacteria over cell monolayers. Next, an agarose overlay (2 ml per well) consisting of serum containing DMEM, 10 μg ml^{-1} gentamicin and 5% low-melting-temperature agarose (Fisher Scientific) was added to each well. Plates were left at room temperature in a tissue culture hood for 10–15 min to allow for the agarose overlay to solidify and then incubated overnight at 37°C and 5% CO_2. The next day, a secondary agarose layer (1 ml per well) containing 10 μg ml^{-1} gentamicin, 5% low-melting-temperature agarose and 0.1% neutral red dye (Sigma) overlay the original layer to assist in visualization of plaques. Plates were then incubated at 37°C and 5% CO_2 and the number of plaques were counted after 24–48 h.

Transfection with cDNA plasmids

Transfections with various Myo10 cDNA plasmid constructs, were accomplished using FuGene6 Transfection Reagent (Roche) or Lipofectin Reagent (Invitrogen) according to the manufacturer's instructions. The GFP-Myo10 plasmid constructs were constructed and transfected as described previously (Bohil *et al*., 2006). The GFP-M10-MyTH4-FERM tail construct (Fig. 7A) was produced using the PCR primers ATAATAAGATCTTACAAGCGGATTCCCATCCTG and

ATAATAAAGCTTTCACCTGGAGCTGCCCTGGC to generate a cDNA that encodes a truncate beginning at Y1521 and ending with the final amino acid R2052 of Myo10. Cells were allowed to incubate at 37°C and 5% CO_2 overnight to allow for uptake. Cells were generally infected at 48 h the time of maximum expression.

Transfection with siRNAs

Transfections with control siRNA (purchased from either Qiagen or Dharmacon) and Myo10 siRNA [purchased from Qiagen as described previously (Zhang *et al*., 2004) or purchased from Dharmacon as catalogue number J-007217-06-0005] were accomplished using the RNAifect Transfection Reagent (Qiagen) according to the manufacturer's instructions. Cells were allowed to incubate at 37°C and 5% CO_2 for 48 h to allow for efficient knock-down of Myo10. All results were assessed by quantitative Western blot analysis (see below).

Western blots

Western blots were performed using cytoplasmic extracts subjected to SDS-PAGE. Confluent monolayers of either HeLa, Cos7 or Caco2 cells were washed once and subsequently scraped in a 150 μl volume of 1× PBS containing 10× protease inhibitor cocktail (Complete Protease Inhibitor Cocktail tablets, Roche). The solution was then passaged several times through a 23- or 25-gauge needle to lyse cells and shear DNA without causing proteolysis to endogenous Myo10 levels. Samples were subjected to SDS-PAGE on 7.5% polyacrylamide gel and transferred to a PVDF membrane (Millipore). A polyclonal Myo10 antibody raised in rabbit was used at a dilution of 1:1000 to probe the membrane (Berg *et al*., 2000) followed by an HRP-conjugated secondary antibody at a dilution of 1:2000. Super Signal West Pico Chemiluminescent Substrate was used for protein detection (Pierce). To verify equal protein loading, the membrane was stripped using Restore Western Blot Stripping Buffer (Pierce) and re-blotted with monoclonal β-actin antibody raised in mouse (Sigma) at a dilution of 1:5000 followed by an HRP-conjugated secondary antibody at a dilution of 1:10 000.

Immunofluorescence and phalloidin stain

For immunofluorescence experiments, HeLa cells infected with *S. flexneri* were treated with 3.7% formaldehyde, then permeabilized with 0.2% Triton X-100 with the exception of ConA staining (see below). A blocking solution (5% fetal bovine serum resuspended in 1× PBS) was then added to cells, followed by primary antibody at a concentration of 1:250. Anti-human Myo10 polyclonal rabbit antibody (Berg *et al*., 2000). Actin filaments were stained using Alexa-conjugated phalloidin as previously described (Sidhu *et al*., 2005). Cell membranes were stained with Alexa-conjugated Concanavilin A (Alexa 488 ConA, Molecular Probes).

Video microscopy

Time-lapse (live) and immunofluorescence (fixed) images were obtained using either a Nikon (Tokyo, Japan) or a Zeiss (Germany) inverted microscope connected to a cooled

charge-coupled device camera (Hamamatsu, model C5985). Images were analysed using AxioVision Release 4.6 image software (Carl Zeiss MicroImaging).

SEM imaging

Cells grown on Thermanox coverslips were fixed in Trumps pH 7.2 (Arch Pathol Lab Med-Vol 100, Aug 1976). The following steps were with the aid of a Pelco Biowave Laboratory Microwave. The samples were washed in PBS and post-fixed with 1% osmium tetroxide. The fixed samples were washed in deionized water and dehydrated in a graded ethanol series. The samples were then dried with a critical point dryer (Balzers CPD 030, NJ) with bone dry carbon dioxide, mounted with carbon double sticky tabs (Ted Pella, Redding, CA) Denton Vacuum Desk II sputter coated with gold-palladium and viewed on a S-4000 field emission SEM (Hitachi High Technologies, American, NJ).

Immunogold-labelled electron micrographs

Shigella-infected HeLa cells on 5 mm round glass coverslips were permeabilized for 2 min at 37°C with PHEM buffer containing 0.75% Triton, protease inhibitors and 1 μM phallacidin. The resultant cytoskeletons were washed with PHEM buffer, fixed with 1% glutaraldehyde in PHEM buffer for 10 min and washed into PBS. Unreacted aldehydes were blocked with a 1 mg ml^{-1} wash of sodium borohydride in PBS and the cytoskeletons were washed extensively in PBS, and placed in PBS containing 1% BSA and 0.001% sodium azide. Coverslips were incubated with rabbit anti-myosin X IgG at a concentration of 10 μg ml^{-1} for 3 h, washed thrice with PBS/BSA solution, incubated with 10 nm goat anti-rabbit IgG-coated gold particles for 3 h, washed thrice with PBS/BSA, thrice with PBS and fixed with 1% glutaraldehyde in PBS for 10 min. The cytoskeletons were washed into distilled water, rapidly frozen on a liquid helium cooled copper block, freeze-dried at −90°C in a Cressington CFE-60 apparatus, and cast with 1.5 nm of tantalumtungsten at 25° with rotation, and 3 nm of carbon at 90° without rotation (Hartwig, 1992).

Statistical analysis

The Mann–Whitney non-parametric unpaired two-tail test was used for assessment of statistical significance.

Supplementary Material

Refer to Web version on PubMed Central for supplementary material.

Acknowledgments

We would like to thank Andrew Thomas for his GFP-Myo10-MyTH4-FERM cDNA construct. This work was funded by RO1 AI034276 and RO1 DC03299.

References

Bennett RD, Mauer AS, Strehler EE. Calmodulin-like protein increases filopodia-dependent cell motility via up-regulation of myosin-10. J Biol Chem. 2007; 282:3205–3212. [PubMed: 17130134]

Bennish ML, Wojtyniak BJ. Mortality due to shigellosis: community and hospital data. Rev Infect Dis. 1991; 13(Suppl. 4):S245–S251. [PubMed: 2047645]

Berg JS, Cheney RE. Myosin-X is an unconventional myosin that undergoes intrafilopodial motility. Nat Cell Biol. 2002; 4:246–250. [PubMed: 11854753]

Berg JS, Derfler BH, Pennisi CM, Corey DP, Cheney RE. Myosin-X, a novel myosin with pleckstrin homology domains, associates with regions of dynamic actin. J Cell Sci. 2000; 113(Part 19):3439–3451. [PubMed: 10984435]

Berg JS, Powell BC, Cheney RE. A millennial myosin census. Mol Biol Cell. 2001; 12:780–794. [PubMed: 11294886]

Bohil AB, Robertson BW, Cheney RE. Myosin-X is a molecular motor that functions in filopodia formation. Proc Natl Acad Sci USA. 2006; 103:12411–12416. [PubMed: 16894163]

Cox D, Berg JS, Cammer M, Chinegwundoh JO, Dale BM, Cheney RE, Greenberg S. Myosin X is a downstream effector of PI(3)K during phagocytosis. Nat Cell Biol. 2002; 4:469–477. [PubMed: 12055636]

Finlay BB, Falkow S. Common themes in microbial pathogenicity revisited. Microbiol Mol Biol Rev. 1997; 61:136–169. [PubMed: 9184008]

Goldberg MB, Theriot JA, Sansonetti PJ. Regulation of surface presentation of IcsA, a *Shigella* protein essential to intracellular movement and spread, is growth phase dependent. Infect Immun. 1994; 62:5664–5668. [PubMed: 7960150]

Gupton SL, Gertler FB. Filopodia: the fingers that do the walking. Sci STKE. 2007; 2007:re5. [PubMed: 17712139]

Hartwig JH. Mechanisms of actin rearrangements mediating platelet activation. J Cell Biol. 1992; 118:1421–1442. [PubMed: 1325975]

Kerber ML, Cheney RE. Myosin-X: a MyTH-FERM myosin at the tips of filopodia. J Cell Sci. 2011; 124:3733–3741. [PubMed: 22124140]

Kerber ML, Jacobs DT, Campagnola L, Dunn BD, Yin T, Sousa AD, et al. A novel form of motility in filopodia revealed by imaging myosin-X at the single-molecule level. Curr Biol. 2009; 19:967–973. [PubMed: 19398338]

Kotloff KL, Winickoff JP, Ivanoff B, Clemens JD, Swerdlow DL, Sansonetti PJ, et al. Global burden of *Shigella* infections: implications for vaccine development and implementation of control strategies. Bull World Health Organ. 1999; 77:651–666. [PubMed: 10516787]

Liu KC, Jacobs DT, Dunn BD, Fanning AS, Cheney RE. Myosin-X functions in polarized epithelial cells. Mol Biol Cell. 2012; 23:1675–1687. [PubMed: 22419816]

Lu Q, Yu J, Yan J, Wei Z, Zhang M. Structural basis of the myosin X PH1N-PH2-PH1C tandem as a specific and acute cellular PI(3,4,5)P3 sensor. Mol Biol Cell. 2011; 22:4268–4278. [PubMed: 21965296]

Mashanov GI, Tacon D, Peckham M, Molloy JE. The spatial and temporal dynamics of pleckstrin homology domain binding at the plasma membrane measured by imaging single molecules in live mouse myoblasts. J Biol Chem. 2004; 279:15274–15280. [PubMed: 14729907]

Meitert T, Pencu E, Ciudin L, Tonciu M, Mihai I, Nicolescu S. Correlation between Congo red binding as virulence marker in *Shigella* species and Sereny test. Roum Arch Microbiol Immunol. 1991; 50:45–52. [PubMed: 1802051]

Oaks EV, Wingfield ME, Formal SB. Plaque formation by virulent *Shigella flexneri*. Infect Immun. 1985; 48:124–129. [PubMed: 3884506]

Plantard L, Arjonen A, Lock JG, Nurani G, Ivaska J, Stromblad S. PtdIns(3,4,5)P is a regulator of myosin-X localization and filopodia formation. J Cell Sci. 2010; 123:3525–3534. [PubMed: 20930142]

Pust S, Morrison H, Wehland J, Sechi AS, Herrlich P. *Listeria monocytogenes* exploits ERM protein functions to efficiently spread from cell to cell. EMBO J. 2005; 24:1287–1300. [PubMed: 15729356]

Rogers MS, Strehler EE. The tumor-sensitive calmodulin-like protein is a specific light chain of human unconventional myosin X. J Biol Chem. 2001; 276:12182–12189. [PubMed: 11278607]

Sansonetti PJ. Microbes and microbial toxins: paradigms for microbial-mucosal interactions III. Shigellosis: from symptoms to molecular pathogenesis. Am J Physiol Gastrointest Liver Physiol. 2001; 280:G319–G323. [PubMed: 11171613]

Sansonetti PJ, Arondel J, Fontaine A, d'Hauteville H, Bernardini ML. OmpB (osmo-regulation) and icsA (cell-to-cell spread) mutants of *Shigella flexneri*: vaccine candidates and probes to study the pathogenesis of shigellosis. Vaccine. 1991; 9:416–422. [PubMed: 1887672]

Sidhu G, Li W, Laryngakis N, Bishai E, Balla T, Southwick F. Phosphoinositide 3-kinase is required for intracellular *Listeria monocytogenes* actin-based motility and filopod formation. J Biol Chem. 2005; 280:11379–11386. [PubMed: 15642729]

Stevens JM, Galyov EE, Stevens MP. Actin-dependent movement of bacterial pathogens. Nat Rev Microbiol. 2006; 4:91–101. [PubMed: 16415925]

Umeki N, Jung HS, Sakai T, Sato O, Ikebe R, Ikebe M. Phospholipid-dependent regulation of the motor activity of myosin X. Nat Struct Mol Biol. 2011; 18:783–788. [PubMed: 21666676]

Watanabe TM, Tokuo H, Gonda K, Higuchi H, Ikebe M. Myosin-X induces filopodia by multiple elongation mechanism. J Biol Chem. 2010; 285:19605–19614. [PubMed: 20392702]

Weber KL, Sokac AM, Berg JS, Cheney RE, Bement WM. A microtubule-binding myosin required for nuclear anchoring and spindle assembly. Nature. 2004; 431:325–329. [PubMed: 15372037]

Wei J, Goldberg MB, Burland V, Venkatesan MM, Deng W, Fournier G, et al. Complete genome sequence and comparative genomics of *Shigella flexneri* serotype 2a strain 2457T. Infect Immun. 2003; 71:2775–2786. [PubMed: 12704152]

Wei Z, Yan J, Lu Q, Pan L, Zhang M. Cargo recognition mechanism of myosin X revealed by the structure of its tail MyTH4-FERM tandem in complex with the DCC P3 domain. Proc Natl Acad Sci USA. 2011; 108:3572–3577. [PubMed: 21321230]

Zeile WL, Purich DL, Southwick FS. Recognition of two classes of oligoproline sequences in profilin-mediated acceleration of actin-based *Shigella* motility. J Cell Biol. 1996; 133:49–59. [PubMed: 8601612]

Zhang H, Berg JS, Li Z, Wang Y, Lang P, Sousa AD, et al. Myosin-X provides a motor-based link between integrins and the cytoskeleton. Nat Cell Biol. 2004; 6:523–531. [PubMed: 15156152]

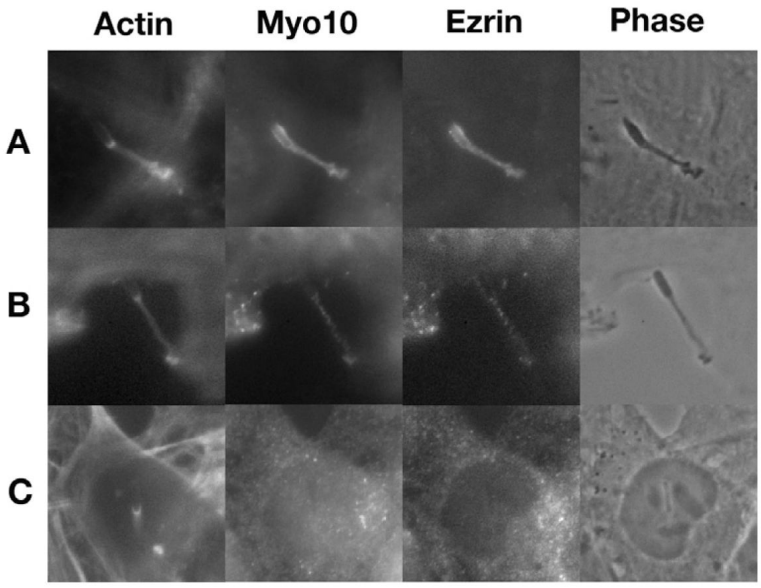

Fig. 1.

Phalloidin, anti-Myo10 antibody, anti-ezrin antibody labelling of *Shigella*-infected HeLa cells.

A. *Shigella*-induced membrane protrusion showing F-actin, Myo10 and host cell membrane (anti-ezrin antibody). The far right phase image shows the bacterium at the tip of the membrane protrusion.

B. A second *Shigella*-induced membrane protrusion. Labelling identical to Fig. 1A.

C. *Shigella* within the cytoplasm of a HeLa cell. Note the F-actin staining, but the absence of anti-Myo10 antibody labelling.

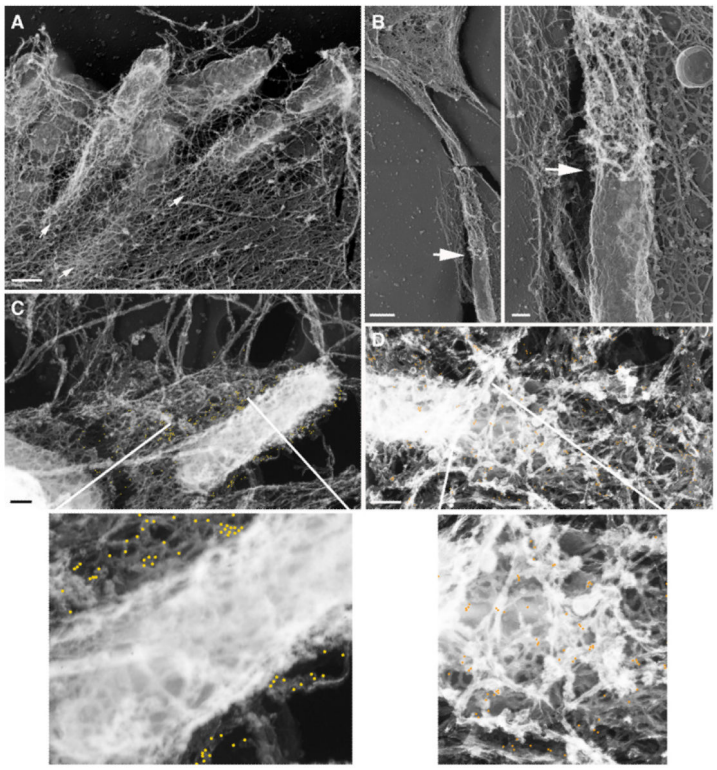

Fig. 2.

Structure of cytoskeletal tails produced by *Shigella* as they move through the cortical cytoplasm of HeLa cells and Myo10 immunogold localization.

A. Multiple bacteria at the cell edge. Some bacteria lack tails while others have tails of highly branched filaments (arrows). The bar is 1 μm.

B. Cytoplasmic stalk from the cell edge produced by a bacterium. The arrow delineates where the actin tail begins on the bacterial surface. The bars are 1 μm (left) and 200 nm (right).

C and D. Localization of Myo10 in *Shigella*-infected HeLa cells using rabbit anti-Myo10 IgG and 10 nm immunogold coated with anti-rabbit IgG. Gold particles have been colourized in yellow to highlight their visibility. The bars are 0.5 μm. (C) Localization of Myo10 on a bacterium lacking a cytoskeletal tail on the edge of the cell. One section of the bacterium has been expanded 3× to better illustrate the location of the gold beads. (D) Localization at the rear of a bacterium with a cytoskeletal tail. A section of the back of the bacterium and F-actin tail has been expanded 3× to better illustrate the concentration of gold beads near the back of the bacterium.

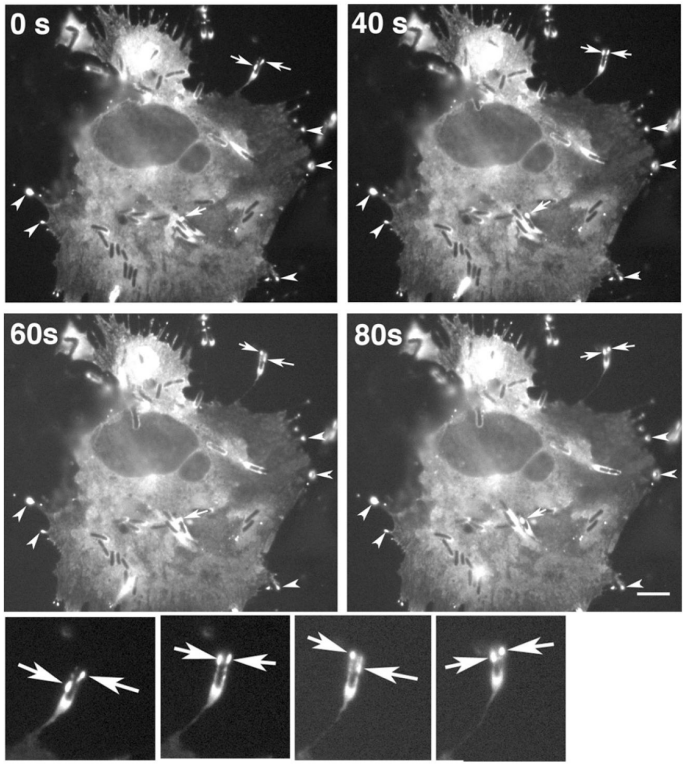

Fig. 3.

Time-lapse video images of GFP-Myo10-transfected PTK2 cells infected with *Shigella*. Images were captured 2 h after initiation of infection. Upper left hand number indicates the time in seconds. Arrows point to clusters of Myo10 that can be seen to cycle along the sides of bacteria forming membrane protrusions. The clearest example of Myo10 cycling is seen in right upper bacterium, and these images are magnified ×2 below the main image, the far left image from frame 0 s and the far right frame 80 s. Note at 0 s, the left sided cluster is below the right cluster. At 40 s, the two clusters are parallel and at 60 s the left cluster is above the right cluster. Note that as Myo10 cycles along the bacterium, the thin stalk connecting the bacterium to the cell body becomes longer, while the length of the bright actin tail does not change. Also note that Myo10 concentrates in the ragged peripheral membrane in the upper region of the cell. Arrowheads point to clusters of Myo10 at the tips of spontaneously formed filopodia that do not contain bacteria. Bar = 10 μm. See supplemental Video S1.

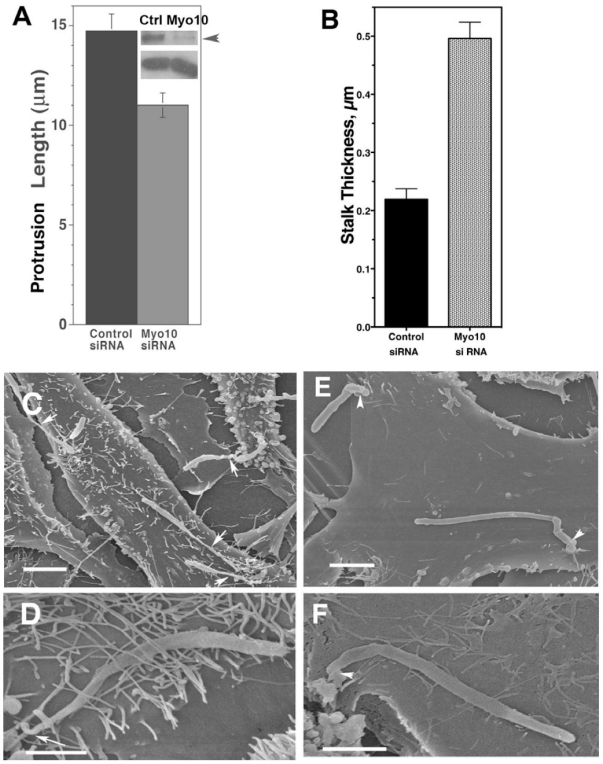

Fig. 4.

Effects of transfection with Myo10 siRNA on *Shigella*-induced membrane protrusions

A. Bar graphs demonstrating the effects of siRNA knock-down of Myo10 on *Shigella*-induced membrane protrusion length. Lengths were measured by fluorescent micrographs of RFP-CAAX-transfected cells (membrane label, see *Experimental procedures*) after formalin fixation of *Shigella*-infected HeLa cells. Bracket represent the SEM of $n = 126$ for control siRNA and $n = 110$ membrane protrusions for Myo10 siRNA-treated HeLa cells fixed 2–3 h after initiation of the *Shigella* infection. Insert shows anti-Myo10 antibody-treated Western blots of extracts from HeLa cells transfected with control and MyoX siRNA for 48 h. The higher-molecular-weight 250 kDa polypeptide is Myo10 (arrowhead), and is decreased by over 90% following Myo10 siRNA treatment. The lower 43 kDa polypeptide, actin, served as a loading control.

B. Bar graphs showing the effects of Myo10 knock-down on membrane protrusion stalk thickness assessed by scanning electron micrographs. (Compare Fig. 4C and D with E and F). The two-dimensional widths of stalks were measured for all membrane protrusions in *Shigella*-infected HeLa cells. Brackets represent the SEM for $n = 54$ membrane protrusions for control cells and $n = 68$ for Myo10 siRNA-treated cells.

C. Scanning EM (low magnification) of infected HeLa cells treated with control siRNA. Note the multiple small dorsal filopodia, as well as the bacteria containing membrane protrusions. The arrows point to the thin stalks connecting the bacteria to the cell body (stalk widths were 0.13, 0.17, 0.17 and 0.17 μm). Bar = 5 μm.

D. Higher magnification of a scanning electron micrograph of infected HeLa cells treated with control siRNA showing a single bacteria containing membrane protrusion connected to the cell body by a narrow stalk (arrow) with a width of 0.14 μm. Note the large number of

spontaneously forming dorsal filopodia as previously observed in uninfected HeLa cells (Bohil *et al*., 2006). Bar = 2 μm.

E. Lower magnification of a scanning electron micrograph of infected HeLa cells treated with Myo10-specific siRNA. Two bacteria containing membrane protrusions are seen, both having thick stalks connecting the bacteria to the cell body (arrowheads) (stalk widths: 0.85 and 0.85 μm). Also note the paucity of spontaneously forming dorsal filopodia, as previously observed when uninfected HeLa cells were treated with siMyo10 RNA (Bohil *et al*., 2006). Bar = 5 μm.

F. Higher magnification of an infected HeLa cell treated with Myo10 siRNA. Arrowhead points to the thick stalk of the bacteria containing membrane protrusion (stalk width: 0.5 μm). Bar = 2 μm.

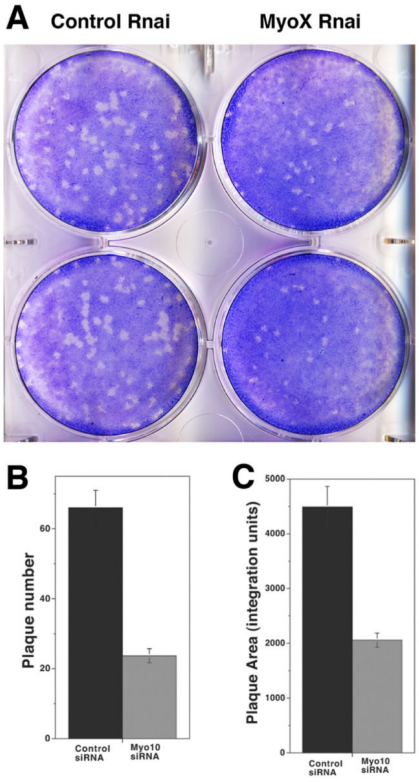

Fig. 5.

Effects of myosin siRNA knock-down on *Shigella* plaque formation.

A. *Shigella*-infected confluent layers of HeLa cells transfected with control siRNA (left) or Myo10 siRNA (right). Dishes are stained blue to make plaques more readily visible. Note the smaller number and decreased diameter of the plaques in the right (Myo10 siRNA) dishes.

B. Bar graph quantifying the number of plaques per dish. The brackets represent the SEM of $n = 4$ separate confluent tissue culture dishes for each condition. Note the marked reduction in plaque number per dish in the Myo10 siRNA-treated HeLa cells.

C. Bar graph quantifying the mean area of the plaques. Brackets represent the SEM of plaques areas from four culture dishes per condition. Combining the plaque number with the plaque areas the total two-dimensional area of tissue cell necrosis was calculated to be reduced by >80% in the Myo10 siRNA as compared with the control siRNA-treated *Shigella*-infected monolayers.

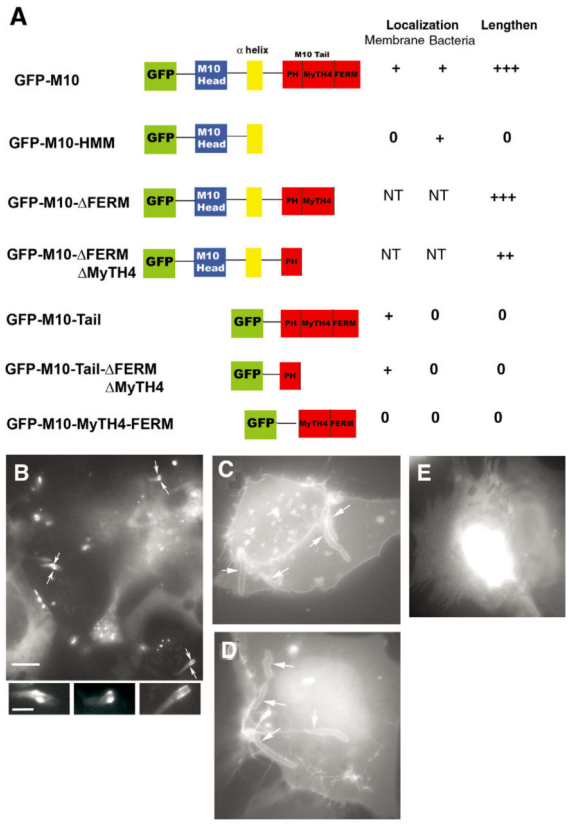

Fig. 6.

Localization of full-length and truncated GFP-Myo10 in *Shigella*-infected Cos7 cells.

A. Schematic diagram of the different GFP constructs transfected into Cos7 cells, a cell line that has low numbers of dorsal filopodia (Bohil *et al*., 2006). A summary of the localization and effects of each construct on *Shigella*-induced membrane protrusion is shown in the right columns.

B. Fluorescence micrograph of HeLa cells transfected with GFP-M10-HMM and infected with *Shigella*. Arrows point to the Myo10-HMM clusters along the sides of the bacteria within membrane protrusions. Below the main image, higher magnification images of the three bacteria-containing membrane protrusions are shown. Of 50 transfected cells containing 83 membrane protrusions, 100% contained HMM. In no case was HMM found around bacteria in the cytoplasm. Note that unlike full-length Myo10 this construct failed to localize to membrane structures, primarily concentrating along the sides of bacteria within membrane protrusions. Bar = 10 μm for the lower magnification and 5 μm for the enlarged images.

C. Fluorescence micrographs of *Shigella*-infected Cos7 cells transfected with the full-length GFP-Myo10 tail. Note that the tail localizes to the peripheral membranes including the bacteria-induced membrane protrusions.

D. Cells transfected with GFP-Myo10-tail-PH missing the MyTH4 and FERM domains. Note that this construct shows very similar localization to the full-length tail.

E. Cells transfected with GFP-Myo10-MyTH4-FERM. The probe is found diffusely throughout the cytoplasm and in the nucleus, but fails to localize to the peripheral membranes. Intracellular bacteria exclude the fluorescent probe. Bar = 10 μm.

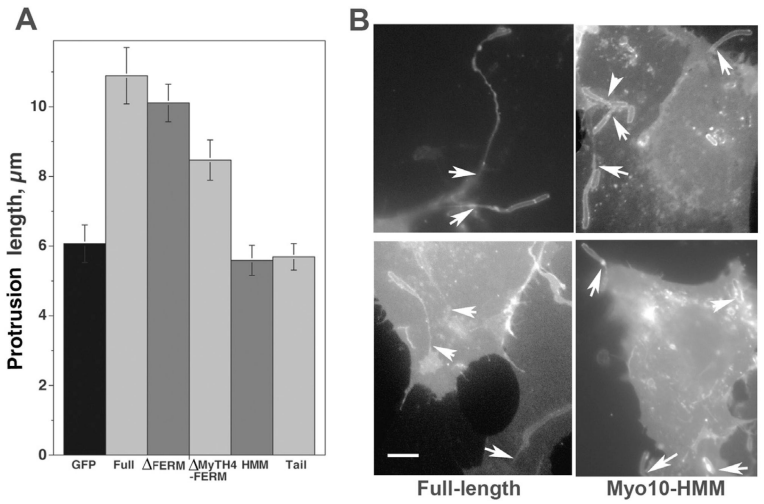

Fig. 7.

Effects of transfecting Cos7 cells with full-length and truncated Myo10 on the length of *Shigella*-induced membrane protrusions.

A. Bar graph showing the mean length of membrane protrusions in Cos7 cells transfected with the constructs depicted in Fig. 6A, as well as RFP-CAAX, a membrane targeting sequence. Cells were then infected with *Shigella* and fixed 2.5 h after initiation of infection. The lengths of all bacteria containing membrane protrusions were measured by fluorescence microscopy (see Fig. 7B). Bars represent the mean length and brackets show the SEM of n = 81–110 membrane protrusions per condition.

B. Fluorescent micrographs using the rhodamine channel to detect RFP-CAAX. Note the membrane protrusions are shorter and the stalks (arrows) significantly thicker in infected cells transfected with GFP-HMM (right), as compared with cells transfected with full-length GFP-Myo10 (left).

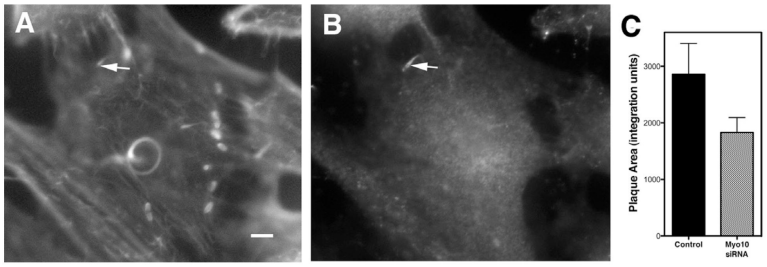

Fig. 8.

Actin filament and Myo10 localization in *Listeria*-infected cells and the effects of Myo10 siRNA on *Listeria* plaque formation.

A. Rhodamine channel – Phalloidin staining of a *Listeria*-infected HeLa cell shows several actin filament tails, two behind bacteria within the cytoplasm and one within a peripheral membrane protrusion (arrow). There are also multiple immobile intracellular bacteria surrounded by actin filaments.

B. Fluorescein channel – Anti-Myo10 staining of the same cell. Myo10 localizes to the bacterium and actin filament tail within the membrane protrusion (arrow) and does not stain any of the bacteria deep within the cytoplasm.

C. Bar graph comparing the mean plaque area of *Listeria*-infected HeLa cell monolayers transfected with a random control siRNA or Myo10-specific siRNA. Brackets show the SEM of $n = 6$ separate dishes for each condition.

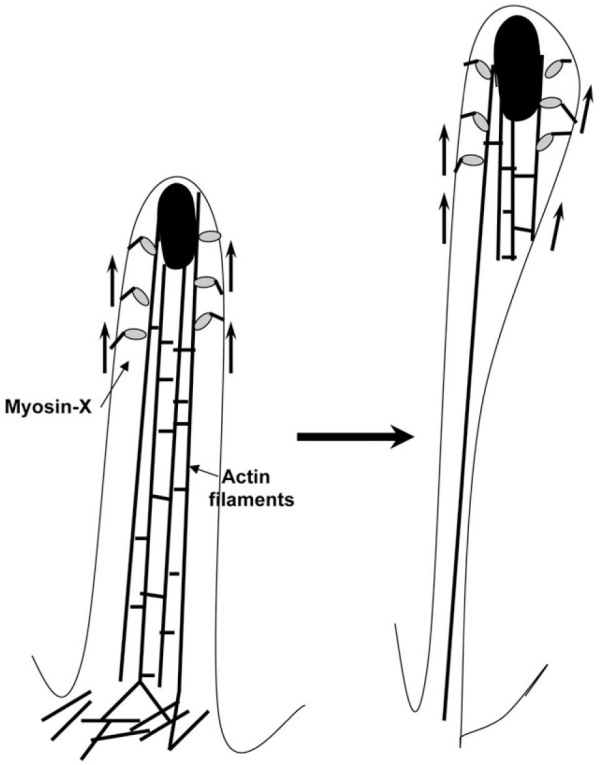

Fig. 9.

Schematic model of how Myo10 enhances the elongation of *Shigella*-induced membrane protrusions. The myosin heads bind to actin filaments on the sides of the bacterium (tip of each protrusion). Arrows parallel to the peripheral membrane point to the direction of membrane movement. For simplicity Myo10 is shown as a monomer rather than as a dimer. The Myo10 tail is linked to the inner leaflet of membrane by the tail-PH domain, and as the myosin heads cycle from 90 degrees to 45 degrees they transport membrane towards the membrane protrusion tip. As the membrane protrusion elongates the stalk progressively thins as the actin filament content decreases near the base of the stalk. The left hand image stalk contains four actin filaments while the right hand image contains a single actin filament. The number of filaments *in vivo* is considerably more; however, this schematic depiction depicts the relative changes F-actin content of the stalk structure.